




## Research Article

# Synthesis and characterization of ceria-coated silica nanospheres: their application in heterogeneous catalysis of organic pollutants

I. Kitsou<sup>1</sup> · M. Arkas<sup>2</sup> · A. Tsetsekou<sup>1</sup> 

Received: 29 August 2019 / Accepted: 31 October 2019 / Published online: 6 November 2019  
© Springer Nature Switzerland AG 2019

## Abstract

The present work investigates the parameters for the successful coating of silicon oxide nanoparticles surface with a homogeneous cerium oxide shell in an effort to develop core–shell nanostructures. For this, spherical silica nanoparticles (~ 300 nm) were developed by a biomimetic approach and their coating with ceria was performed through a precipitation method. Several processing conditions, such as the precipitation pH, the cerium precursor concentration and the treatment of silica cores (i.e., their use either as-received after their biomimetic formation, or after their calcination followed by surface modification), were examined and optimized. The as-obtained powder material was characterized by scanning electron microscopy, high-resolution transmission electron microscopy, Fourier transform infrared spectroscopy, X-ray diffraction analysis, N<sub>2</sub> adsorption and UV–Vis reflectance spectroscopy. The analysis revealed the formation of spherical core–shell nanostructures bearing a uniform shell layer of crystalline cerium oxide around each silica core which after calcination at 600 °C was comprised of cubic CeO<sub>2</sub> nanocrystals with sizes ranging between 2 and 6 nm. The material with the optimum core–shell structure and pure cerium dioxide were studied in terms of their catalytic reduction activity over 4-nitrophenol to 4-aminophenol.

**Keywords** Core–shell · Cerium oxide · Silicon oxide · Environmentally friendly procedure · Catalytic reduction

## 1 Introduction

Recent technological breakthroughs and the desire for new features have created a huge demand for new materials. Many of the usual materials, such as metals, ceramics or plastics, cannot fulfill all of the technology requirements for many novel and demanding applications. In recent years, the research for the preparation of core–shell nanoparticles with a well-defined structure has attracted considerable interest due to their excellent physical and chemical properties, such as optical, electrical, thermal,

mechanical, magnetic and catalytic ones, compared to pure materials. [1, 2].

Nanomaterials consisting of a core and a shell are commonly referred as core–shell nanomaterials/nanoparticles (CSNs or CSNp) [3, 4]. Core–shell nanomaterials are extremely functional materials with modified properties [5]. The majority of the CSNs are manufactured in order to combine two materials—and therefore two or more properties in one structure. Thereby, the new structure is characterized by the properties of both core and shell, giving a variety of new potentials and countless combinations [6]. Their production can be realized either in a

**Electronic supplementary material** The online version of this article (<https://doi.org/10.1007/s42452-019-1613-y>) contains supplementary material, which is available to authorized users.

✉ A. Tsetsekou, [athtse@metal.ntua.gr](mailto:athtse@metal.ntua.gr) | <sup>1</sup>School of Mining and Metallurgical Engineering, National Technical University of Athens, Iroon Polytechniou 9, 157 80 Zografos, Athens, Greece. <sup>2</sup>Institute of Nanoscience and Nanotechnology, NCSR “Demokritos”, 15310 Aghia Paraskevi, Attiki, Greece.



SN Applied Sciences (2019) 1:1557 | <https://doi.org/10.1007/s42452-019-1613-y>

one-step process where the core particles are synthesized in situ, this being followed by the coating of the shell material, or in a two-step process. In the latter, the core is firstly synthesized and then the synthesis of the shell follows [5, 7] employing several synthetic procedures such as sol–gel [8], microemulsion [9], polymerization [10] or deposition–precipitation [11]. By this way, various types of materials can be combined such as dielectric materials, metals and semiconductors, where the core consists of one of the materials and the shell of another or the same material [5, 12].

There are manifold purposes of coating the core particle, for instance, surface modification, the ability to increase the functionality, stability and dispersibility, the controlled release of the core, the reduction in consumption of precious materials and so forth [6, 13]. Apart from the improved material properties, core/shell materials are also significant from a financial viewpoint. For example, a precious material can be coated over an inexpensive material in order to reduce its consumption as opposed to making the same size structure composed of the pure precious material [4, 5, 14, 15].

Cerium dioxide or ceria ( $\text{CeO}_2$ ) is considered as a very useful material as it can be used in various applications such as polishing material [16] or solid oxide fuel cell electrolyte [17]. Moreover, it is not toxic, a fact that makes it useful in optoelectronics and photocatalysis [18]. Owing to the high oxygen storage capacity and the ability to stabilize the dispersed metal cation species, ceria has attracted researchers' attention finding many applications in environmental catalysis [19]. Environmental pollution is a major issue and has attracted the interest of researchers, primarily because of adverse effects on human health and all living organisms. Industry causes many environmental problems, releasing a wide range of toxic substances into the environment [20]. Heterogeneous catalysis, as a means of anti-pollution, has also attracted much interest and has become an emergent technology approach for a sustainable environment, such as the removal of organic pollutants from aqueous effluents [21].

It is well known that size, shape, surface state and crystallinity are crucial factors for the catalytic performance of nanomaterials. Due to their tendency for aggregation during the catalytic process, their catalytic activity and stability are declined [22].

Therefore, different approaches have been investigated to control these properties. Conventional production methods such as precipitation and sol–gel usually result in large particles (about 50 nm), whereas the thermal degradation of cerium salts leads to particles of high porosity and specific surface area, but the control of particle size and morphology is very limited [23]. Many researchers wishing to overcome these problems have developed

various methods of preparing silica–ceria core–shell particles as silica can offer many advantages such as good dispersion, narrow size distribution and controlled particle size [24–29]. However, in previous studies [30], the final particles showed intense agglomeration due to the formation of hydrogen bonds because of the presence of water during the precipitation process. In addition, the resulting suspension contained both coated silica particles and pure ceria particles. Thus, the development of core–shell structures which leads to good dispersion, narrow size distribution and controlled particle size will favor the catalytic process.

In the present study, the main objective is to develop a core–shell material comprising a uniform nano- $\text{CeO}_2$  shell onto silica cores produced by an environmentally friendly method, as well as to reduce the cost of the final material as cerium oxide is an expensive material. The experimental procedure took place at ambient temperature, while the neutralizing agent for the precipitation of cerium oxide on the silica surface was a polymer–water solution. Finally, the optimum core–shell structure and the pure  $\text{CeO}_2$  were studied for their catalytic properties by their ability to catalyze the reduction of 4-nitrophenol to 4-aminophenol in the presence of sodium borohydride. The results showed that the development of core–shell structure affects the catalytic performance of  $\text{CeO}_2$ .

## 2 Materials and methods

### 2.1 Materials

Tetraethyl orthosilicate (TEOS, 98%) was used as a precursor for the silica nanoparticles, and hyperbranched poly(ethylene)imine was used to modify the surface of the silica with the amine groups. Cerium (III) nitrate hexahydrate (99%) was used as a precursor for the ceria shell layer. 4-Nitrophenol (Fluka) was used as the organic pollutant, and sodium borohydrate ( $\text{NaBH}_4$ , 99%) was used as the reducing agent. All materials, except 4-nitrophenol, were purchased from Sigma-Aldrich and used without further purification.

### 2.2 Synthesis of the core–shell nanoparticles

Firstly, silica cores were prepared through the hydrolysis–condensation reaction of silicic acid in the presence of hyperbranched poly(ethylene)imine [31]. To create the core–shell structure, the silica cores were calcined at 800 °C for 3 h under airflow and then they were redispersed in water.

Then, silicas' surface was modified with HBPEI ( $\text{SiO}_2/\text{HBPEI}$ ) and the cores were redispersed in water again.

Following that, cerium (III) nitrate hexahydrate (in a percentage of 25, 33 or 50 w/w on silica amount) was added and the sol was kept under stirring for approximately 30 min. Finally, an appropriate amount of 1:10 w/v HBPEI/water sol was added dropwise in order to increase the pH value up to 10.5. The resulting suspension was kept under stirring for 24 h in order for the reactions to be completed. This was followed by the centrifugation and washing with water steps, drying with the freeze drying (FD) method and finally calcination at 600 °C for 2 h. The as-obtained samples are described in Table 1.

### 2.3 Characterization techniques

The morphology of the core-shell structures as well as of pure SiO<sub>2</sub> and CeO<sub>2</sub> was examined via transmission electron microscopy (TEM) with a high-resolution transmission electron microscope (HRTEM, JEOL 2100 HR) which is equipped with a JED-2300T energy-dispersive X-ray spectrometer and a digital scanning image observation device (STEM, JEOL EM 24511 SIOD). Scanning electron microscopy (SEM) images were recorded with JEOL 6380LV. X-ray diffraction (XRD) patterns were obtained on a diffractometer (Bruker D8 Focus) with nickel-filtered CuK $\alpha$  radiation ( $k = 1.5406 \text{ \AA}$ , 40 kV, 40 mA), in the range of 10–80°. FTIR spectroscopy was also conducted using a Nicolet Magna-IR spectrometer 550. N<sub>2</sub> adsorption/desorption measurements were taken using a Micromeritics ASAP 2000 apparatus, and the surface area was calculated by the BET equation. A UV-Vis spectrophotometer (Hitachi U-3010) was used in order to obtain diffuse reflectance spectra.

#### 2.3.1 4NP reduction catalysis

The catalytic properties of the material with the optimum core-shell structure and of pure CeO<sub>2</sub> were examined through the reduction of 4-nitrophenol (Fluka) to 4-aminophenol in the presence of NaBH<sub>4</sub> (sodium borohydride 99%, Sigma-Aldrich) as the reductant under room temperature. In aqueous solutions of 4NP in a concentration of 4 ppm, 1.6 g/l NaBH<sub>4</sub> and 0.2 g/l of catalyst were added. The progress of the reaction was monitored using UV-Vis spectroscopy (UV-Vis Spectrometer, Cary

100). The samples were filtered and measured in the range of 200–800 nm at different times.

## 3 Results and discussion

### 3.1 Silica-ceria core-shell nanoparticles

The preparation of core-shell nanoparticles is a very difficult process as various difficulties are encountered, namely the agglomeration of the cores, the tendency to create separate particles from the coating material instead of coating the cores, the incomplete coating and the difficult control of the reaction degree [5].

Firstly, an attempt was made for biomimetic synthesis, where the cerium precursor was added to the silica nanospheres without being calcined and chemically surface-modified. However, inhomogeneities in the final coating as well as the creation of independent ceria nanoparticles were observed (Fig. S1). A pH study was also conducted, using phosphate buffer at various pH values but without leading to the desired result (Fig. S2). For the above reasons, the nanospheres were calcined in order to remove any free amino groups from the surface and then they were subjected to surface chemical modification using HBPEI. In order to simplify the process as well as to minimize the use of harmful substances, the process was carried out in an aqueous medium and at ambient temperature. In similar studies [26, 27, 32, 33], part or the whole reaction was carried out at higher temperature (70–100 °C) as well as with the use of toxic agents such as nitric acid or organic solvents.

The development of the shell was carried out through precipitation on the surface of silica which bears free amino groups. Initially, the cerium ions are bound by the amino groups of HBPEI present on the silica surface. With the addition of the polymer solution, a gradual increase in pH was observed accompanied by a color change. It has been reported that the formation of CeO<sub>2</sub> from nitrate baths proceeds through intermediate steps that involve at first the formation of unstable metal-polymer complexes followed at intermediate pH values by the precipitation of the white trivalent cerium hydroxide. With the further increase in pH, the Ce(III) ion starts being oxidized into Ce(IV) forming again stable complexes with the polymer amine groups and thus being redissolved. Finally, at the elevated pH of 10.5 hydration and dehydration reactions follow leading sequentially to the formation of intermediate Ce(IV) species up to the final cubic nano-CeO<sub>2</sub> that finally forms after a 24-h stirring period (Fig. 1) [34–37].

**Table 1** Codes and w/w ratios of the precursors for the final synthesized materials

Sample code	w/w Ce(NO <sub>3</sub> ) <sub>3</sub> ·6H <sub>2</sub> O/ SiO <sub>2</sub> /HBPEI ratio
ScP25%CeP	0.25:1
ScP33%CeP	0.33:1
ScP50%CeP	0.5:1

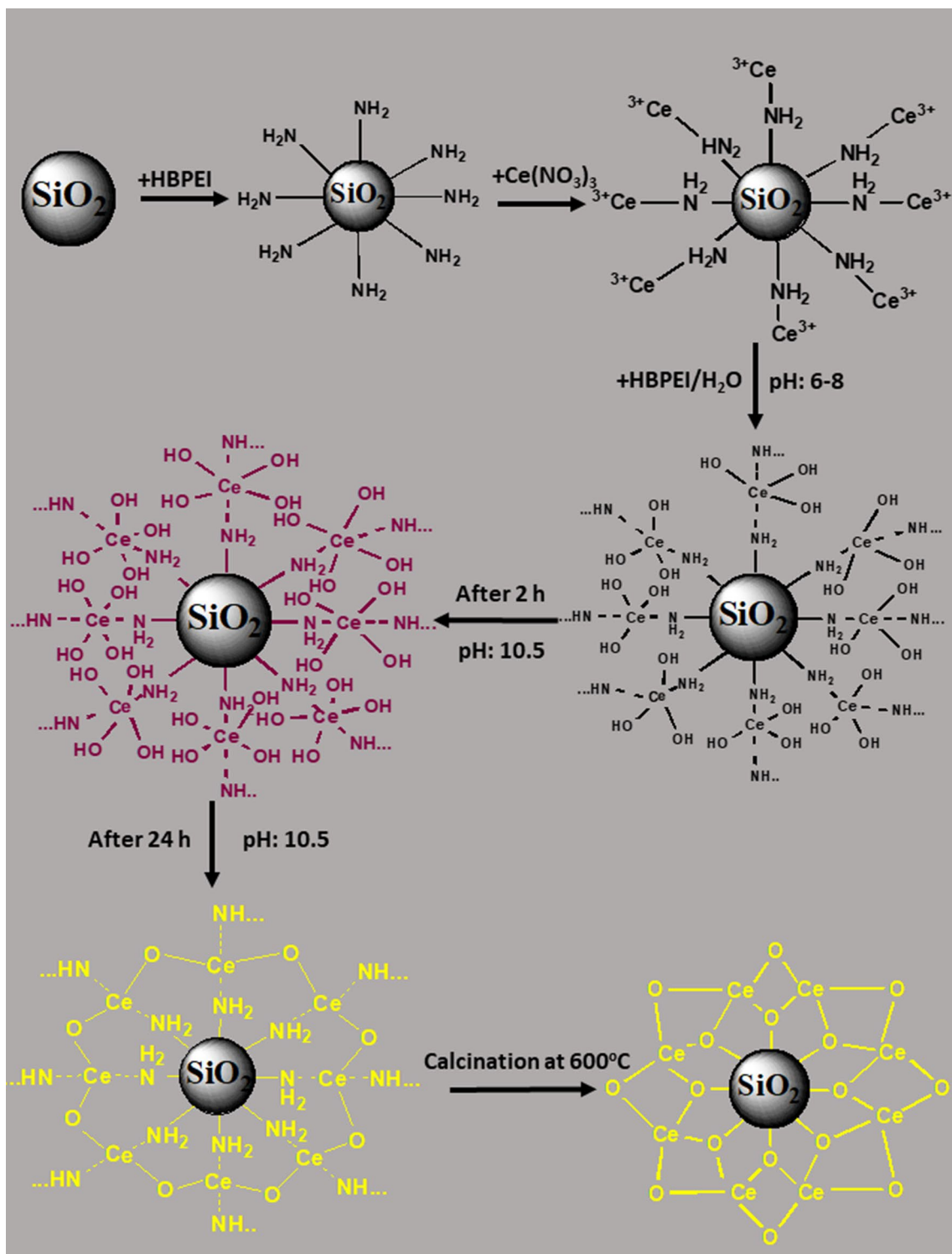


Fig. 1 The formation process for the ceria-coated silica spheres

### 3.2 Morphology of silica cores, cerium oxide and silica–ceria nanoparticles

In order to confirm the synthesis of ceria shell on the

silica surface, HRTEM analysis was performed. Figure 2a, b presents the SEM and TEM images of silica cores. It can be seen that the bare silica particles have a smooth surface with a mean size at around 300 nm. A HRTEM



**Fig. 2** SEM image (a), TEM image (b) and SAED pattern (c) of bare SiO<sub>2</sub> cores. TEM images (d, f) and SAED pattern (e) of CeO<sub>2</sub> after calcination at 600 °C

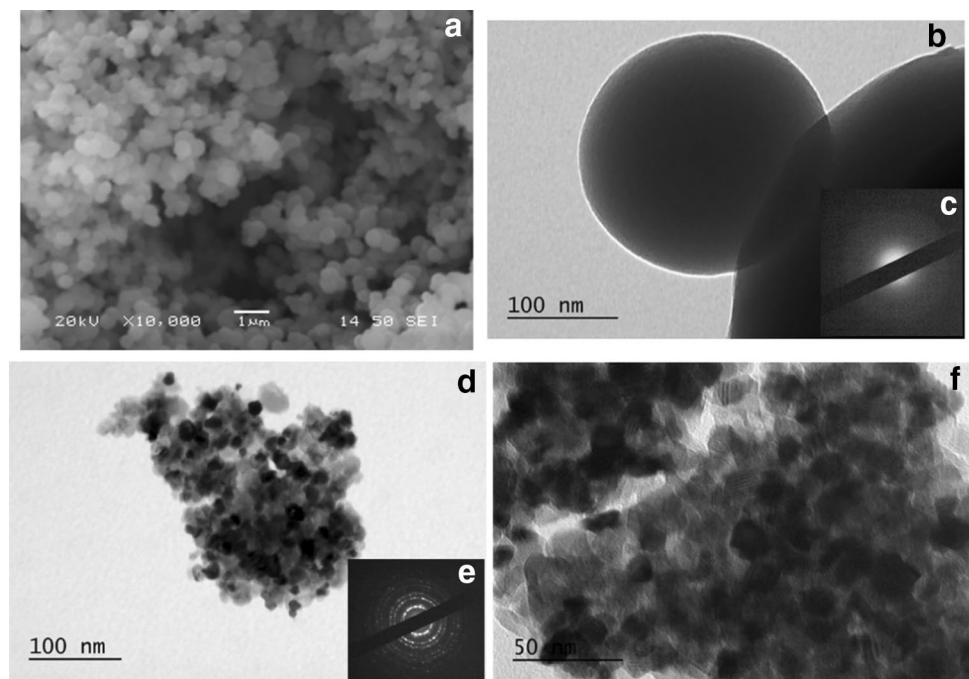
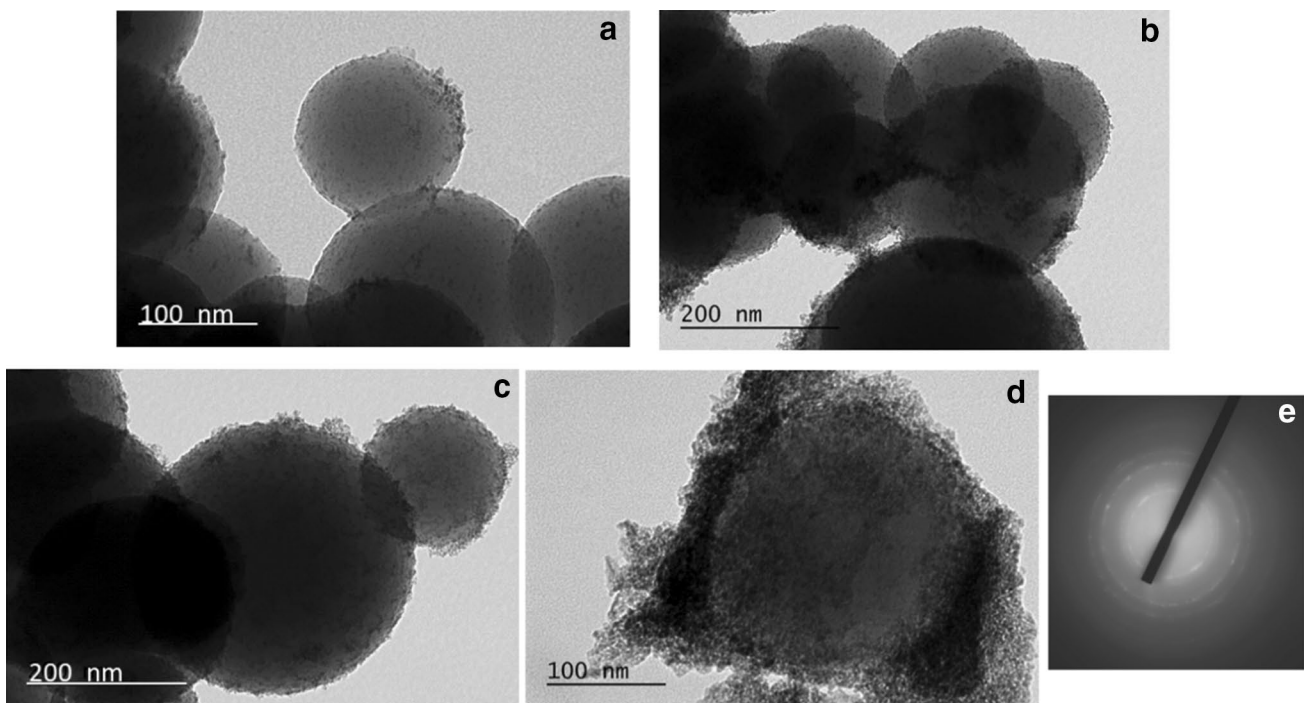


image of the microstructure of pure cerium dioxide is presented in Fig. 2d. The material consists of uniform, almost cubic-shaped grains. The average grain size, calculated using the Image Pro program, was estimated at around 10–20 nm. Further, the selected area electron diffraction pattern (Fig. 2e) in combination with the results

of X-ray diffraction analysis proved that the final material is nanocrystalline.

Figure 3 shows the HRTEM micrographs of the ceria-coated silica particles prepared using 25, 33 and 50% w/w cerium nitrate on the silica cores' amount. From the TEM images, it is clear that a distinctive crystalline (as shown



**Fig. 3** TEM image (a) of ScP25%CeP, TEM images (b, c) and SAED pattern (e) of ScP33%CeP, TEM image (d) of ScP50%CeP

by SAED analysis, Fig. 3e) ceria shell was formed on silica surface, the quality of which, however, depends on ceria precursor quantity employed. More specifically, in the case of using the low precursor quantity of 25% w/w on silica (Fig. 3a), the coating is successful with all the ceria materials being formed onto silica surface. However, the surface coverage is incomplete presenting many gaps. Instead, when the cerium nitrate quantity was increased to 33% w/w (Fig. 3b, c), the silica particles are completely coated with a uniform and very successful ceria layer. Finally, in the case of using 50% w/w cerium nitrate/silica cores, an inhomogeneous and thick ceria coating along with the formation of separate ceria nanoparticles is observed (Fig. 3d).

Comparing the pure ceria material to that formed on silica cores, it should be pointed out that the ceria of the shell material presents a significantly reduced particle size. In particular, after calcination at 600 °C, the size of cerium oxide in the core-shell material varies between 2 and 6 nm, whereas that of the pure cerium oxide was 10–20 nm. The significantly reduced size was achieved possibly due to two key reasons. Firstly, the presence of the SiO<sub>2</sub>/HBPEI cores facilitates the nucleation rate. Secondly, the good dispersion of the CeO<sub>2</sub> particles on the silica cores leads to the reduction in the grain growth during the final calcination process.

In addition, the percentage of CeO<sub>2</sub> in each core-shell structure was calculated using the EDS data and Eq. 1:

$$\%CeO_2 = \frac{gr_{CeO_2}}{gr_{CeO_2} + gr_{SiO_2}} * 100 \tag{1}$$

With the use of STEM and EDS, a number of measurements for separate core-shell nanoparticles were taken. An average % estimation of the measurements is given in Table 2.

### 3.3 XRD measurements

The phase composition of pure ceria as well as that of silica-ceria core-shell nanoparticles was investigated by XRD. Figure 4 shows the XRD pattern of CeO<sub>2</sub> powder after calcination at 600 °C where the peaks of the cubic structure of cerium dioxide are evident [(111), (200), (220), (311), (222), (400), (331) and (420)] (JCPDS No. 34-0394).

**Table 2** % CeO<sub>2</sub> content of each silica-ceria core shell structure

Sample code	% CeO <sub>2</sub>
ScP25%CeP	2.2 ± 0.5
ScP33%CeP	3.3 ± 0.5
ScP50%CeP	5.0 ± 1.0

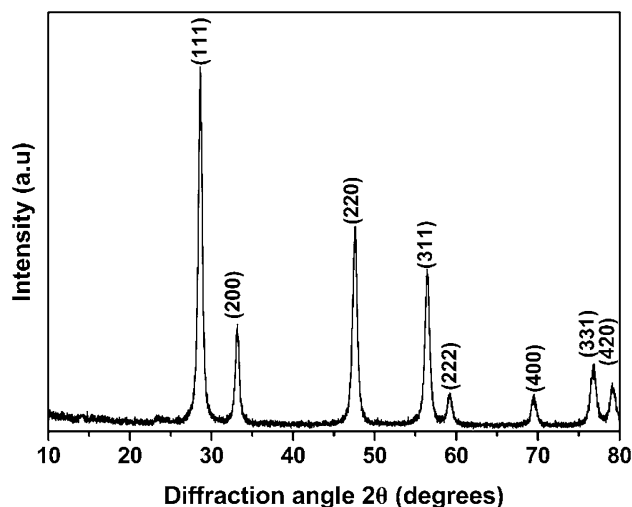


**Fig. 4** XRD pattern of CeO<sub>2</sub> after calcination at 600 °C

The XRD patterns of the core-shell materials (Fig. 5), combined with the results of the selective area electron diffraction pattern and the EDS analysis, confirmed the shell creation since the main peaks [(111), (200), (220), (311), (222), (400), (331) and (420)] of the cubic structure of cerium dioxide (JCPDS No. 34-0394) are presented. As shown in Fig. 5, increasing the weight ratio of Ce(NO<sub>3</sub>)<sub>3</sub>·6H<sub>2</sub>O/SiO<sub>2</sub>/HBPEI from 0.25:1 to 0.33:1 and finally to 0.5:1, the intensity of ceria peaks is also increased. Further, these XRD patterns present a broad peak at about 22 degrees, which corresponds to the amorphous structure of silica [38, 39].

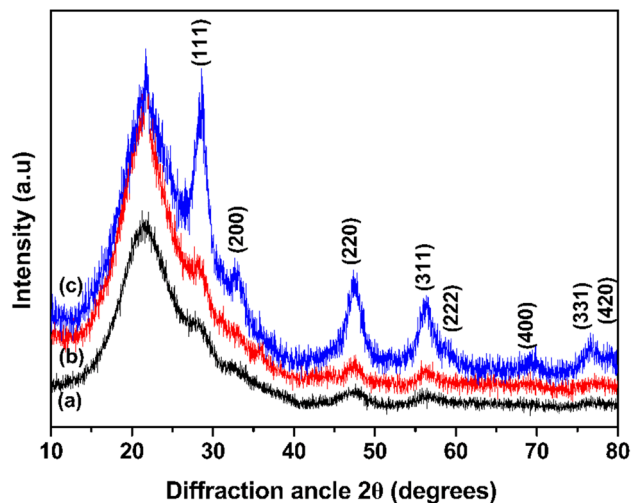


**Fig. 5** XRD patterns of the core-shell structures: (a) ScP25%CeP, (b) ScP33%CeP and (c) ScP50%CeP

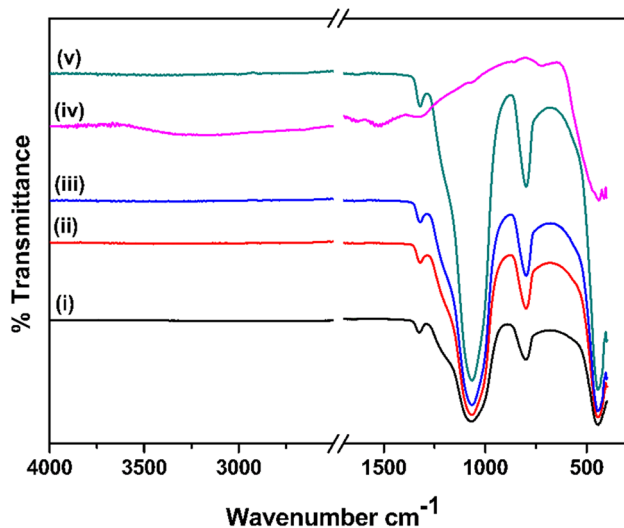


**Fig. 6** FTIR spectra of the silica nanospheres (i), cerium oxide (iv) and core-shell structures ScP25%CeP (ii), ScP33%CeP (iii) and ScP50%CeP (v)

### 3.4 FTIR analysis

Further analysis was performed using Fourier transform (FTIR) infrared spectroscopy. As shown in Fig. 6, no change is detected by increasing the percentage of cerium nitrate in the final material. The peaks at 1066, 797 and 443  $\text{cm}^{-1}$  are attributed to stretching and bending vibrations of Si–O–Si bonds [31, 40, 41], indicating the condensation of silanols to Si–O–Si bonds and the formation of the silica network. The presence of  $\text{CeO}_2$  is confirmed by the peaks at around 405  $\text{cm}^{-1}$  which are attributed to Ce–O bonds [38, 42, 43].

### 3.5 $\text{N}_2$ adsorption analysis

Based on the physicochemical analysis results that have been described above, the material with the optimal coating, i.e., ScP33%CeP, was selected for further analysis. Measurements of the specific surface area of the core-shell material as well as of the pure materials that formed the core and the shell were taken. The  $\text{N}_2$  sorption-desorption isotherms of  $\text{CeO}_2$ ,  $\text{SiO}_2$  and ScP33%CeP are shown in Fig. 7. As it is evident from the IUPAC classification [44], cerium dioxide is a mesoporous material (type IV), and it has a hysteresis loop corresponding to H2 class [45]. The specific surface area of the cerium oxide was recorded at 48.7  $\text{m}^2/\text{g}$ .  $\text{SiO}_2$  cores and ScP33%CeP core-shell material, as shown in Fig. 7, are non-porous materials with a low specific surface area of 25.3 and 27.5  $\text{m}^2/\text{g}$ , respectively. Therefore, it can be concluded that by preparing a new core-shell structure, the specific surface area of the final material is smaller compared to that of pure  $\text{CeO}_2$ . This is

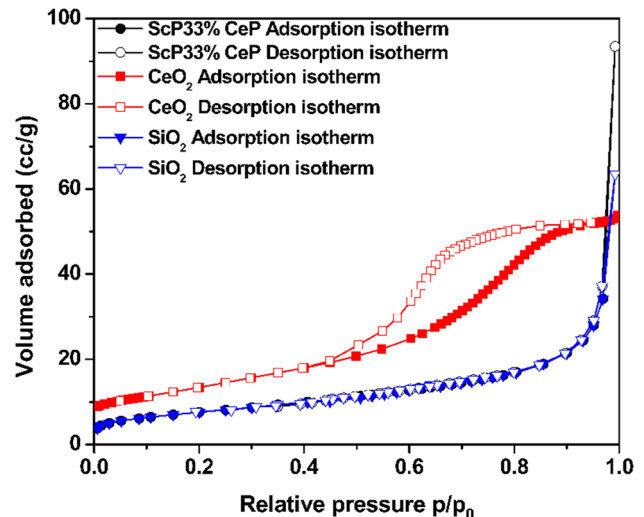


**Fig. 7** Adsorption and desorption isotherms of ScP33%CeP,  $\text{CeO}_2$  and  $\text{SiO}_2$

expected given the small amount and the low thickness of the material deposited on the surface of much larger silica cores having a surface area of  $\sim 25 \text{ m}^2/\text{g}$ .

### 3.6 UV-Vis measurements

Diffuse reflectance spectroscopy was performed in order to estimate the band gaps of the ScP33%CeP,  $\text{CeO}_2$  and  $\text{SiO}_2$ . A plot of the absorption function  $[F(R) \times E]^{1/2}$  versus  $E$  (eV) is depicted in Fig. 8b, where  $F(R) = (1 - R)^2/2R$  is the Kubelka–Munk function expressed through the measured diffuse reflectance  $R$  of the materials and  $E$  is the electromagnetic wave energy. The band gaps were estimated by extrapolating the linear section of the absorption function and measuring the value at its intersection with the energy axis, e.g., at zero absorption [46–48].

The absorption spectrum of cerium dioxide, as well as the value of the energy band gap  $E_{\text{bg}} = 2.53 \text{ eV}$ , coincides with the literature data on doped  $\text{CeO}_2$  [49] as the usual  $E_{\text{bg}}$  value for ceria is 3.1–3.3 eV [50–52]. Therefore, it can be concluded that the experimental process described above leads to the preparation of  $\text{CeO}_2$  with a sufficiently reduced energy band gap. As it is evident and consistent with the literature [53, 54], the reflection spectrum for pure  $\text{SiO}_2$ , given in Fig. 8a, exhibits negligible absorption only in the ultraviolet region. Instead, the pure  $\text{CeO}_2$  as well as the core-shell material ScP33%CeP absorbs in both the visible and ultraviolet regions. The measurement of the energy gap of  $\text{SiO}_2$  material due to the very low absorption was not reliable, but in the literature it is given at around 9 eV [55]. Comparing the spectra and the energy gap values of pure  $\text{CeO}_2$  and the core-shell material ScP33%CeP, a change in absorbance after the creation

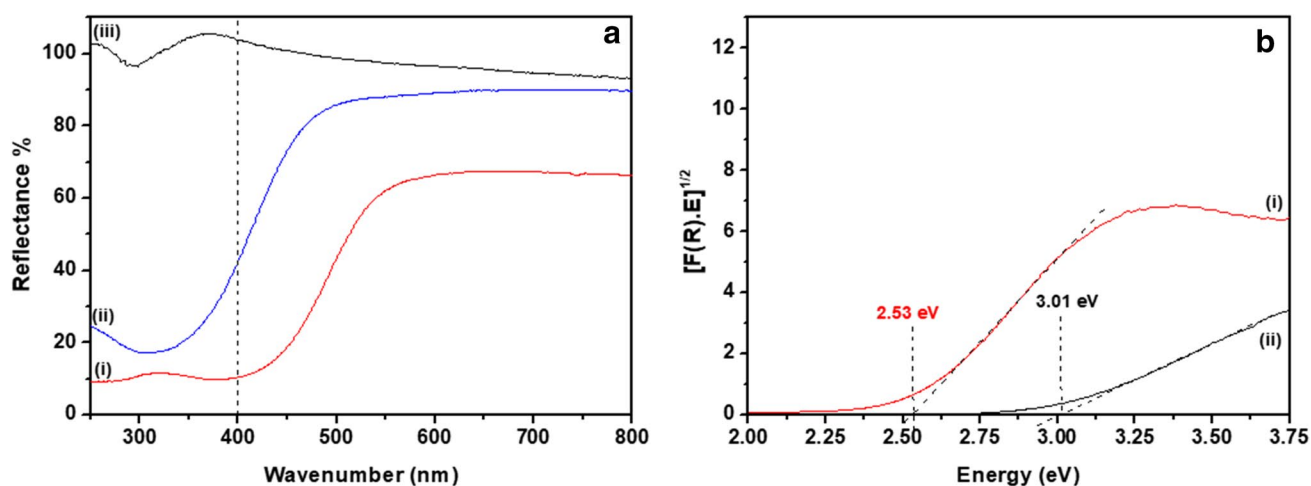


**Fig. 8** a Reflectance spectra of CeO<sub>2</sub> (i), ScP33%CeP (ii) and SiO<sub>2</sub> (iii), b absorption function  $[f(R) \times E]^{1/2}$  versus energy E for CeO<sub>2</sub> (i) and ScP33%CeP (ii)

of the new core–shell structure is shown. In particular, the absorption spectrum of the core–shell structure is shifted to smaller wavelengths, while it exhibits a higher reflectance (Fig. 8a). The core–shell material has a higher energy gap value of 3.01 eV than that of pure CeO<sub>2</sub>, which could be attributed to the smaller particle size of CeO<sub>2</sub> [56] in the core–shell structure, as it was observed by TEM analysis.

#### 4 Catalytic activity of ScP33%CeP and CeO<sub>2</sub> for 4NP reduction

The industrial manufacture of pharmaceuticals, agrochemicals and dyes produces nitro-aromatic compounds which are harmful to the environment and eventually to humans. These compounds can be reduced into their amine form, which is non-toxic, with the appropriate catalytic process. The nanoreactor with the optimum core–shell structure, i.e., ScP33%CeP as well as the pure ceria, was examined for the catalytic reduction of 4-nitrophenol to 4-aminophenol in the presence of NaBH<sub>4</sub> as the reducing agent at ambient conditions. As shown in Fig. 9, the absorption peak at 317 nm indicates the presence of the organic pollutant, whereas the reduction of 4NP to 4-nitrophenolate ion, after the addition of the reducing agent, is indicated by the peak shift to 400 nm. This peak is gradually decreased over the time and a new peak at ~300 nm appeared indicating the reduction of 4NP to 4AP [57–59].

The concentration of NaBH<sub>4</sub> exceeded the concentration of 4-NP. The high concentration of the reducing agent results in high pH values and as a consequence in deceleration of the degradation of the borohydride ions. In addition, the oxidation of the 4-aminophenol product is prevented due to the presence of free hydrogen from the

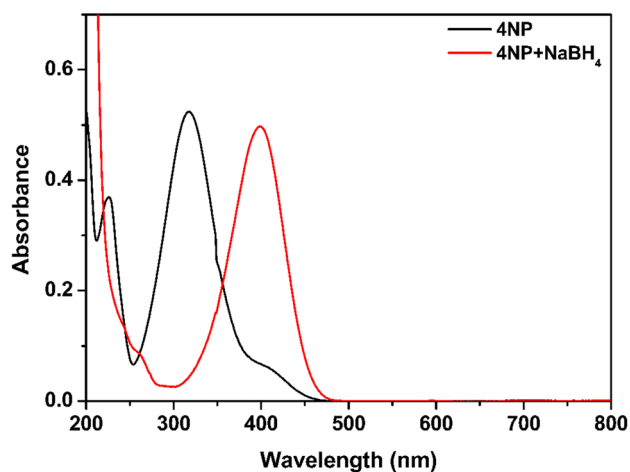


**Fig. 9** UV-Vis spectra of 4NP before and after adding NaBH<sub>4</sub>

borohydride ions which purged out the air. After the addition of the catalyst, NaBH<sub>4</sub> and 4-NP are absorbed onto the catalysts surface and the reduction process is started by transferring electrons from the BH<sub>4</sub><sup>-</sup> donor to the 4NP acceptor. At this point, it must be pointed out that in the absence of catalyst the reaction was not taken place even after 24 h [39, 57–59]. Consequently, the presence of the catalytic nanoreactor is crucial.

Figure 10a, b presents UV-Vis spectra of ScP33%CeP and CeO<sub>2</sub>. As shown in Fig. 10c, ScP33%CeP achieved 47.8% conversion of the organic pollutant 4-NP whereas pure CeO<sub>2</sub> achieved only 8.5% conversion. Therefore, it can be concluded that the new structure favors the catalytic performance as it is far exceeding that of pure cerium dioxide. The higher rate of conversion of the core–shell material can be attributed to the smallest



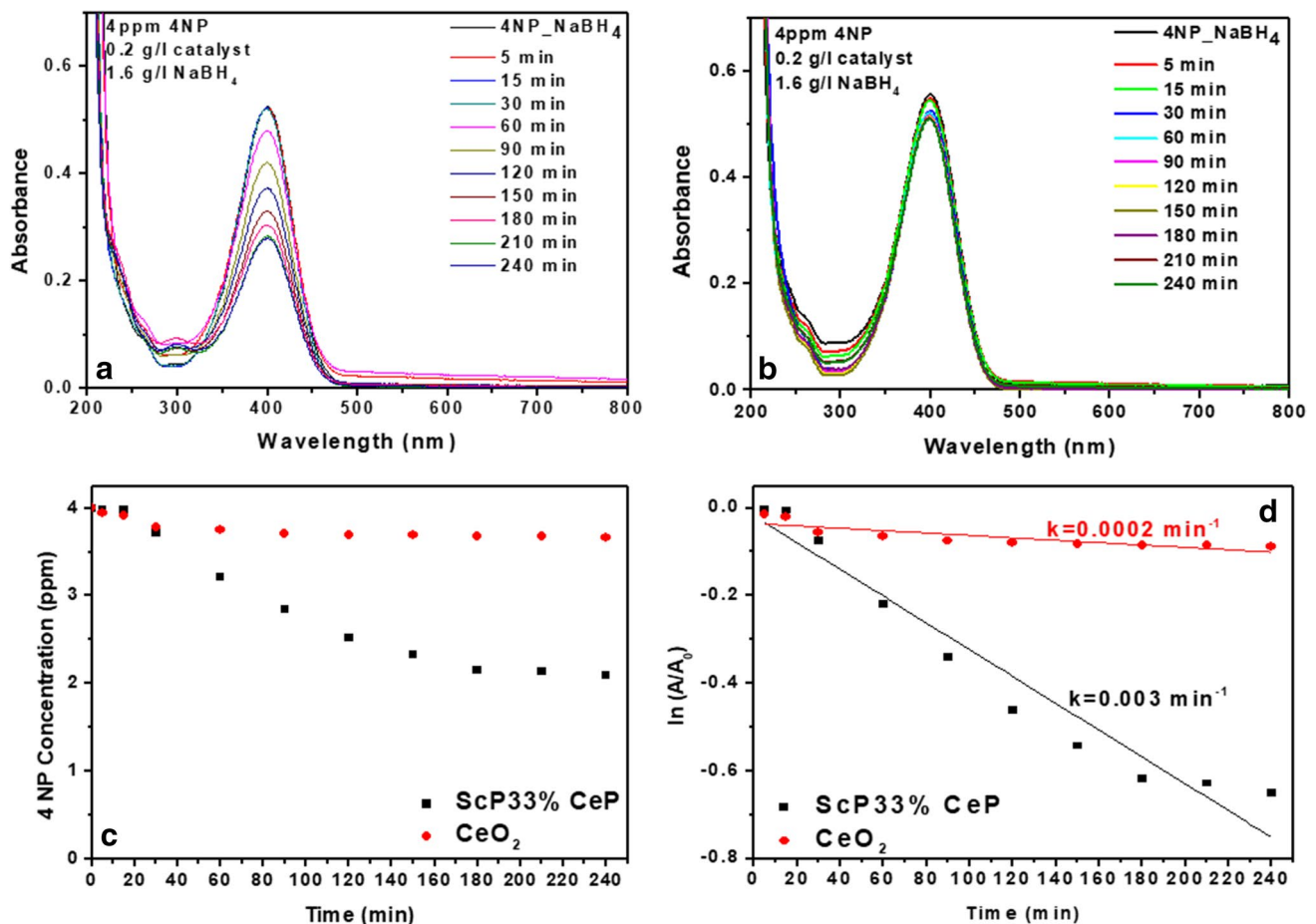


**Fig. 10** Time versus UV-Vis absorption spectra for the catalytic reduction of 4NP by  $\text{NaBH}_4$  in the presence of ScP33%CeP (a) and  $\text{CeO}_2$  (b), 4NP concentration versus time plots of 4NP reduction by

$\text{NaBH}_4$  in the presence of ScP33%CeP and  $\text{CeO}_2$  (c), comparative plots of  $\ln(A/A_0)$  for ScP33%CeP and  $\text{CeO}_2$  toward the reduction of 4NP (d)

particle size and the good dispersion of  $\text{CeO}_2$  on the silica surface so no aggregates are present and thus more reactive sites are offered [60]. Significant benefit of core-shell structures, as the ScP33%CeP, is their bigger particle size, which simplifies their separation and collection by a heterogeneous system.

The catalytic reduction of 4NP to 4-AP in excess of  $\text{NaBH}_4$  is commonly described by a first-order rate kinetic equation with respect to nitrophenolate ion concentration. Hence, the apparent rate constant ( $k$ ) for each material was estimated from the slope of the straight lines in Fig. 10d [57–59]. The degradation rate for the core-shell structure was estimated at  $0.003 \text{ min}^{-1}$ , whereas that for the pure cerium oxide was much lower ( $0.0002 \text{ min}^{-1}$ ) in accordance with the conversion rates discussed above. Furthermore, in both cases, an induction time ( $t_0$ ) for the first 15 min is observed, indicating the surface atoms' of the nanoparticle reorganization in order to be activated before the beginning of the reaction [61].

Further studies concerning the amount of the catalyst were conducted for the core-shell structure and pure ceria, and the results are presented in Table 3. As it can be observed, with the increase in the catalyst amount, the % conversion and as a consequence the rate constant  $k$  are reduced in both cases. At this point, it must be pointed out that in the case of pure  $\text{CeO}_2$ , the rate constants for catalyst concentrations 0.4 and 0.6 g/l were not estimated due to the very low % conversion of 4NP

**Table 3** % Conversion and the respective rate constants of the catalytic systems

Catalyst concentration (g/l)	ScP33%CeP		$\text{CeO}_2$	
	% Conversion	$k \times 10^{-2}$ ( $\text{min}^{-1}$ )	% Conversion	$k \times 10^{-2}$ ( $\text{min}^{-1}$ )
0.2	47.8	0.306	8.5	0.02
0.4	28.9	0.135	3.8	–
0.6	8.7	0.00195	3.8	–

to 4-AP. The decrease in the % conversion is possibly ascribed to the aggregation of the particles due to the higher amount of catalyst and hence the reduction in the total active surface area of the material. Generally, in a heterogeneous system, the dispersion of the catalyst in the aqueous system may influence the rate of the reaction [62, 63].

From the above results, it is evident that the development of a new  $\text{SiO}_2@\text{CeO}_2$  core-shell structure promotes the catalytic activity of ceria. Using only a small amount of  $\text{CeO}_2$  as a shell on silica cores, the catalytic activity of the final material is five times higher than that of pure  $\text{CeO}_2$ .

## 5 Conclusions

Uniform  $\text{SiO}_2@\text{CeO}_2$  core-shell nanoparticles were prepared through an environmentally friendly chemical precipitation method. The whole process was carried out with the objective to establish an economical and environmentally friendly process, so the temperature used was that of the environment, while only distilled water was employed as solvent. Important parameters proved the calcination and surface modification of silica cores by HBPEI, the w/w  $\text{Ce}(\text{NO}_3)_3 \cdot 6\text{H}_2\text{O}/\text{SiO}_2/\text{HBPEI}$  ratio employed (with the optimum one being at 0.33:1) and the  $\text{CeO}_2$  precipitation pH which was adjusted again by HBPEI. By this way, homogeneous, spherical  $\text{SiO}_2@\text{CeO}_2$  core-shell nanoparticles of a mean size at 300 nm comprising a uniform ceria layer were developed. The  $\text{CeO}_2$  shell on top of  $\text{SiO}_2$  cores had a very fine nanostructure consisted of nanocrystals of the cubic  $\text{CeO}_2$  with sizes ranging between 2 and 6 nm. Measurements on pure ceria particles (not on top of silica cores) developed using the same procedure revealed significantly higher particle size, about 10–20 nm, compared to that of ceria particles in the core-shell material. The  $\text{N}_2$  porosimetry study showed that the material with the optimum coating had a reduced specific surface area compared to pure cerium dioxide, i.e., 27.5  $\text{m}^2/\text{g}$  versus 48.7  $\text{m}^2/\text{g}$  due to the much smaller amount of ceria particles impacted on much larger silica cores. The catalytic activity of the core-shell structure over 4-nitrophenol was found at 47.8% conversion, while that of the pure  $\text{CeO}_2$  was 8.5%, indicating the high efficacy of the core-shell structure and the good dispersion of  $\text{CeO}_2$  particles on the silica cores.

## Compliance with ethical standards

**Conflict of interest** The authors declare that they have no conflict of interest.

## References

- Bala H, Zhang Y, Ynag H, Wang C, Li M, Lv X, Wang Z (2007) Preparation and characteristics of calcium carbonate/silica nanoparticles with core-shell structure. *Colloids Surf A: Physicochem Eng Asp* 294:8–13
- Hwang HS, Bae JH, Kim HG, Lim KT (2010) Synthesis of silica-polystyrene core-shell nanoparticles via surface thiol-lactam initiated radical polymerization. *Eur Polym J* 46:1654–1659
- Thatai S, Khurana P, Boken J, Prasad S, Kumar D (2014) Nanoparticles and core-shell nanocomposite based new generation water remediation materials and analytical techniques: a review. *Microchem J* 116:62–76
- Gawande BM, Goswami A, Asefa T, Guo H, Biradar VA, Peng D-L, Zboril R, Varma SR (2015) Core-shell nanoparticles: synthesis and applications in catalysis and electrocatalysis. *R Soc Chem*. <https://doi.org/10.1039/c5cs00343a>
- Chaudhuri RG, Paria S (2012) Core/shell nanoparticles: classes, Properties, synthesis mechanisms, characterization, and applications. *Chem Rev* 112:2373–2433
- Srdić VV, Mojić B, Nikolić M, Ognjanović S (2013) Recent progress on synthesis of ceramics core/shell nanostructures. *Process Appl Ceram* 7:45–62
- Wei S, Wang Q, Zhu J, Sun L, Lin H, Guo Z (2011) Multifunctional composite core-shell nanoparticles. *Nanoscale* 3:4474–4502
- Milde M, Dembski S, Osvet A, Batentschuk M, Winnacker A, SEXTL G (2014) Polymer-assisted sol-gel process for the preparation of photostimulable core/shell structured  $\text{SiO}_2/\text{Zn}_2\text{SiO}_4:\text{Mn}^{2+}$  particles. *Mater Chem Phys* 148:1055–1063
- Saboor FH, Khodadadi AA, Mortazavi Y, Asgari M (2017) Microemulsion synthesized silica/ZnO stable core/shell sensors highly selective to ethanol with minimum sensitivity to humidity. *Sens Actuat, B* 238:1070–1083
- Dresco PA, Zaitsev VS, Gambino RJ, Chu B (1999) Preparation and properties of magnetite and polymer magnetite nanoparticles. *Langmuir* 15:1945–1951
- Peng X, Peng K, Huang J (2017) Synthesis and magnetic properties of core-shell structured Finemet/Ni-Zn ferrite soft nanocomposites by co-precipitation. *J Alloys Compd* 691:165–170
- Michael Fleming S, Tarun Mandal K, David Walt R, Assembly Nanosphere-Microsphere (2001) Methods for Core-shell materials preparation. *Chem Mater* 13:2210–2216
- He B, Zhao Q, Zeng Z, Wang X, Han S (2015) Effect of hydrothermal reaction time and calcination temperature on properties of  $\text{Au}@\text{CeO}_2$  core-shell catalyst for CO oxidation at low temperature. *J Mater Sci* 50:6339–6348
- Kalele S, Gosavi SW, Urban J, Kulkarni SK (2006) Nanoshell particles: synthesis, properties and applications. *Curr Sci* 91:1038–1052
- Jankiewicz BJ, Jamiola D, Choma J, Jaroniec M (2012) Silica-metal core-shell nanostructures. *Adv Colloid Interface Sci* 170:28–47
- Cook LM (1990) Chemical processes in glass polishing. *J Non-Cryst Solids* 120:152–171
- Atkinson A, Barnett S, Gorte RJ, Irvine JTS, McEvoy AJ, Mogensen M, Singhal SC, Vohs J (2004) Advanced anodes for high-temperature fuel cells. *Nat Mater* 3:17–27
- Usharani S, Rajendran V (2016) Optical, magnetic properties and visible light photocatalytic activity of  $\text{CeO}_2/\text{SnO}_2$  nanocomposites. *Eng Sci Technol Int J* 19:2088–2093
- Pang J, Wenting L, Cao Z, Xu J, Li X, Zhang X (2018) Mesoporous  $\text{Cu}_2\text{O}-\text{CeO}_2$  composite nanospheres with enhanced catalytic activity for 4-nitrophenol reduction. *Appl Surf Sci* 439:420–429

20. Khan SB, Faisal M, Rahman MM, Jamal A (2011) Exploration of CeO<sub>2</sub> nanoparticles as a chemi-sensor and photo-catalyst for environmental applications. *Sci Total Environ* 409:2987–2992
21. Lei W, Zhang T, Gu L, Liu P, Rodriguez AJ, Liu G, Liu M (2015) Surface structure-sensitivity of CeO<sub>2</sub> nanocrystals in photocatalysis and enhancing the reactivity with nanogold. *ACS Catal* 5:4385–4393
22. Liu B, Yu S, Wang Q, Hu W, Jing P, Liu Y, Jia W, Liu Y, Liu L, Zhang J (2013) Hollow mesoporous ceria nanoreactors with enhanced activity and stability for catalytic application. *Chem Commun* 49:3757–3759
23. Li YX, Zhou XZ, Wang Y, You XZ (2004) Preparation of nano-sized CeO<sub>2</sub> by mechanochemical reaction of cerium carbonate with sodium hydroxide. *Mater Lett* 58:245–249
24. StÖber W, Fink A, Bohn E (1968) Controlled growth of monodisperse silica spheres in the micron size range. *J Colloid Interface Sci* 26:62–69
25. Masui T, Tategaki H, Imanaka N (2004) Preparation and characterization of SiO<sub>2</sub>-CeO<sub>2</sub> particles applicable for environment-friendly yellow pigments. *J Mater Sci* 39:4909–4911
26. Zhang Z, Liu W, Zhua J, Song Z (2010) Synthesis, characterization of ceria-coated silica particles and their chemical mechanical polishing performance on glass substrate. *Appl Surf Sci* 257:1750–1755
27. Munusamy P, Sanghavi S, Varga T, Suntharampillai T (2014) Silica supported ceria nanoparticles: a hybrid nanostructure to increase stability and surface reactivity of nano-crystalline ceria. *RSC Adv* 4:8421–8430
28. Borujeny ER, Dawkins K, Li P, Xu Z, Cadien K (2016) Ceria coated silica particles: one step preparation and settling behavior under the influence of colloidal and hydrodynamic interactions. *Mater Chem Phys* 173:467–474
29. Chen Y, Zuo C, Zefeng Li, Chen A (2018) Design of ceria grafted mesoporous silica composite particles for high-efficiency and damage-free oxide chemical mechanical polishing. *J Alloys Compd* 736:276–288
30. Li JG, Ikegami T, Lee JH, Mori T (2001) Characterization and sintering of nanocrystalline CeO<sub>2</sub> powders synthesized by a mimic alkoxide method. *Acta Mater* 49:419–426
31. Arkas M, Tsiourvas D (2009) Organic/inorganic hybrid nanoparticles based on hyperbranched poly(ethyleneimine) encapsulated into silica for the sorption of toxic metal ions and polycyclic aromatic hydrocarbons from water. *J Hazard Mater* 170:35–42
32. Oh M-H, Lee J-S, Gupta S, Chang F-C, Singh RK (2010) Preparation of monodispersed silica particles coated with ceria and control of coating thickness using sol-type precursor. *Colloids Surf A: Physicochem Eng Asp* 355:1–6
33. Yu L, Liu W-L, Zhang Z-F, Song Z-T (2015) Synthesis of colloid silica coated with ceria nano-particles 4 with the assistance of PVP. *Chin Chem Lett* 26:700–704
34. Hamlaoui Y, Pedraza F, Remazeilles C, Cohendoz S, Rébéré C, Tifouti L, Creus J (2009) Cathodic electrodeposition of cerium-based oxides on carbon steel from concentrated cerium nitrate solutions. Part I. Electrochemical and analytical characterization. *Mater Chem Phys* 113:650–657
35. Martínez L, Román E, de Segovia JL, Poupard S, Creus J, Pedraza F (2011) Surface study of cerium oxide based coatings obtained by cathodic electrodeposition on zinc. *Appl Surf Sci* 257:6202–6207
36. Tok AIY, Du SW, Boey FYC, Chong WK (2007) Hydrothermal synthesis of CeO<sub>2</sub> nano-particles. *J Mater Process Technol* 190:217–222
37. Kitsou I, Roussi E, Tsetsekou A (2017) Synthesis of aqueous nano-dispersed nanocrystalline ceria suspensions by a novel organic/inorganic precipitation method. *Ceram Int* 43:3861–3865
38. Song X, Jiang N, Li Y, Xu D, Qiu G (2008) Synthesis of CeO<sub>2</sub>-coated SiO<sub>2</sub> nanoparticle and dispersion stability of its suspension. *Mater Chem Phys* 110:128–135
39. Kitsou I, Panagopoulos P, Maggos Th, Arkas M, Tsetsekou A (2018) Development of SiO<sub>2</sub>@TiO<sub>2</sub> core-shell nanospheres for catalytic applications. *Appl Surf Sci* 441:223–231
40. Motahari S, Abolghasemi A (2015) Silica aerogel-glass fiber composites as fire shield for steel frame structures. *J Mater Civ Eng* 27:04015008/1-7
41. Tang X, Sun A, Chu C, Yu M, Ma S, Cheng Y, Guo J, Xu G (2017) A novel silica nanowire-silica composite aerogels dried at ambient pressure. *Mater Des* 115:415–421
42. Kargar H, Ghazavi H, Darroudi M (2015) Size-controlled and bio-directed synthesis of ceria nanopowders and their in vitro cytotoxicity effects. *Ceram Int* 41:4123–4128
43. Panahi-Kalamuei M, Alizadeh S, Mousavi-Kamazani M, Salavati-Niasari M (2015) Synthesis and characterization of CeO<sub>2</sub> nanoparticles via hydrothermal route. *J Ind Eng Chem* 21:1301–1305
44. Brunauer S, Deming L, Deming W, Teller E (1940) Multimolecular adsorption of gases on silica gel. *J Am Chem Soc* 62:1723–1732
45. Gregg SJ (1982) Adsorption surface area and porosity, 2nd edn. Academic Press Inc., London
46. Kubelka P, Munk F (1931) An article on optics of paint layers. *Z Tech Phys* 12:593–608
47. Morales AE, Mora ES, Pal U (2007) Use of diffuse reflectance spectroscopy for optical characterization of un-supported nanostructures. *Rev Mexicana Fis* 53:18–22
48. Murphy AB (2007) Band-gap determination from diffuse reflectance measurements of semiconductor films, and application to photoelectrochemical water-splitting. *Sol Energy Mater Sol Cells* 91:1326–1337
49. Jorge AB, Sakatani Y, Boissiere C, Laberty-Roberts C, Sauthier G, Fraxedas J, Sanchez C, Fuertes A (2012) Nanocrystalline N-doped ceria porous thin films as efficient visible-active photocatalysts. *J Mater Chem* 22:3220–3226
50. Zhou S-S, Liu S-Q (2017) Photocatalytic reduction of CO<sub>2</sub> based on CeO<sub>2</sub> photocatalyst loaded with imidazole-fabricated N-doped graphene and Cu(II) as cocatalysts. *Photochem Photobiol Sci* 16:1563–1569
51. Babitha KK, Sreedevi A, Priyanka KP, Sabu B, Varghese T (2015) Structural characterization and optical studies of CeO<sub>2</sub> nanoparticles synthesized by chemical precipitation. *Indian J Pure Appl Phys* 53:596–603
52. You D, Pan B, Jiang F, Zhou Y, Su W (2016) CdS nanoparticles/CeO<sub>2</sub> nanorods composite with high-efficiency visible-light-driven photocatalytic activity. *Appl Surf Sci* 363:154–160
53. Bachan N, Asha A, Jothi Jeyarani W, Arun Kumar D, Merline Shyla J (2015) A Comparative investigation on the structural, optical and electrical properties of SiO<sub>2</sub>-Fe<sub>3</sub>O<sub>4</sub> core-shell nanostructures with their single components. *Acta Metall Sin (Engl Lett)* 28:1317–1325
54. Li W, Wang S, He S, Wang J, Guo Y, Guo Y (2015) Enhanced photoluminescence from CdS with SiO<sub>2</sub> nanopillar arrays. *Sci Rep* 5:11375. <https://doi.org/10.1038/srep11375>
55. Tao J, Chai JW, Zhang Z, Pan JS, Wang SJ (2014) The energy-band alignment at molybdenum disulphide and high-k dielectrics interfaces. *Appl Phys. Lett* 104:232110. <https://doi.org/10.1063/1.4883865>
56. Lin K-F, Cheng H-M, Hsu H-C, Lin L-J, Hsieh W-F (2005) Band gap variation of size-controlled ZnO quantum dots synthesized by sol-gel method. *Chem Phys Lett* 409:208–211
57. Srisombat L, Nonkumwong J, Suwannarat K, Kuntalue B, Anant S (2017) Simple preparation Au/Pd core/shell nanoparticles for 4-nitrophenol reduction. *Colloids Surf A* 512:17–25
58. Zhao Y, Wu Z, Wang Y, Yang C, Li Y (2017) Facile fabrication of polystyrene microsphere supported gold-palladium alloy

- nanoparticles with superior catalytic performance for the reduction of 4-nitrophenol in water. *Colloids Surf A*. 529:417–424
59. Wang Z, Xu C, Li X, Liu Z (2015) In situ green synthesis of Ag nanoparticles on tea polyphenols-modified graphene and their catalytic reduction activity of 4-nitrophenol. *Colloids Surf A*. 485:102–110
60. Ullah S et al (2015) Enhanced photocatalytic properties of core@shell SiO<sub>2</sub>@TiO<sub>2</sub> nanoparticles. *Appl Catal B* 179:333–343
61. Aditya T, Pal A, Pal T (2015) Nitroarene reduction: a trusted model reaction to test nanoparticle catalyst. *Chem Commun* 51:9410–9431
62. Deshmukh SP, Dhokale RK, Yadav HM, Achary SN, Delekar SD (2013) Titania-supported silver nanoparticles: an efficient and reusable catalyst for reduction of 4-nitrophenol. *Appl Surf Sci* 273:676–683
63. Nezamzadeh-Ejhieh A, Khorsandi S (2014) Photocatalytic degradation of 4-nitrophenol with ZnO supported nano-clinoptilolite zeolite. *J Ind Eng Chem* 20:937–946

**Publisher's Note** Springer Nature remains neutral with regard to jurisdictional claims in published maps and institutional affiliations.